



Cite this: DOI: 10.1039/d5dt01390a

Porphyrin-functionalized glassy carbon electrodes for electrochemical water splitting†

Neidy Ocuane,¹ Nasim Jafari, Jonathan J. Calvillo Solis,² Manuel Saucedo and Dino Villagrán¹*

Herein, we electrografted the free-base 5,10,15,20-tetrakis(4-aminophenyl)porphyrin, (H₂TAPP) and the cobalt-based porphyrin (CoTAPP) onto the surface of glassy carbon electrodes (GCE) which results in a H₂TAPP-GCE and CoTAPP-GCE polymer, respectively. Electropolymerization forms a stable, covalently bonded network, enhancing the electrochemically active surface area (to 47.7 cm², 29.2 cm², respectively) and lowering the charge transfer resistance during OER and HER based on EIS data. H₂TAPP-GCE exhibits a Tafel slope of 113 mV dec⁻¹ for HER, while CoTAPP-GCE achieves 80 mV dec⁻¹ for OER. The overpotentials are 511 mV (HER) and 540 mV (OER), with both electrodes remaining stable over 20 hours.

Received 12th June 2025,
Accepted 14th July 2025

DOI: 10.1039/d5dt01390a

rsc.li/dalton

Introduction

Hydrogen, known for its high energy density (120 MJ kg⁻¹), and carbon-free nature, has been identified as a promising power alternative energy source.^{1–3} It can be generated through electrochemical water splitting with two half-reactions: hydrogen evolution reaction (HER), and oxygen evolution reaction (OER), which require two and four electrons, respectively.⁴ Thermodynamically water electrolysis requires 1.23 V vs. RHE. Nonetheless, water splitting exhibits sluggish kinetics requiring electrocatalysts to speed up the reaction. Benchmark materials consist of noble metals such as Pt, RuO₂, and IrO₂, however, their practical application is hindered by the cost, scarcity, and corrosion.^{5,6} Therefore, the development of efficient and cost-effective non-noble metal-based catalysts is a key research focus.⁷

Porphyryns are a class of macrocycles that in their metal-free or metalated forms exhibit vibrant colors, multi-electron redox chemistry, and the ability to electrochemically generate H₂ and O₂.^{8,9} Under acidic conditions, the pyrrole rings and N lone pairs in the core of metal-free porphyryns act as active sites for H₂ generation.^{10,11} In metalated porphyryns, the central metal ion (in which the axial positions are often available for coordination) is the active site for the generation of metal-oxo species for OER or metal hydride during HER.^{12–14} Our research group has been investigating stabilization strategies of molecular catalysts such as intercalation and porphyrin polymerization, demonstrating improved stability and

encouraging overpotentials.^{8–10,15} Another method to stabilize molecular catalysts is through electrochemical synthesis of electrocatalytic materials onto electrode surfaces, which ensures strong chemical binding. Common electrochemical synthesis strategies are high-temperature sintering, solvent thermal, and vapor deposition.^{16–18} On the other side, electrografting of molecular catalysts onto surfaces can create electrochemically modified electrodes (ECME) with polymeric structures, enhancing their application in energy conservation.^{19,20} The *in situ* reduction of catalyst materials onto glassy carbon electrodes (GCEs) is considered efficient, economical, and rapid.²¹

In this study, we show the electrografting of both *meso*-tetra(4-aminophenyl)porphyrin (H₂TAPP) and cobalt tetra(4-aminophenyl)porphyrin (CoTAPP) onto GCE. This process was performed by the electrochemical reduction of the respective porphyrin diazonium salts generated *in situ* to create strongly bonded polymeric films. The modified electrodes reveal significant improvements in both HER and OER compared to unmodified GCE. These findings contribute to the advancement of ECME, offering the potential for scalable and efficient water-splitting technologies.

Results and discussion

The synthesis of H₂TAPP and CoTAPP was performed as previously described,⁸ and used without further purification for the electrografting purpose. The UV-Vis spectrum of H₂TAPP (Fig. S1†) exhibits a characteristic Soret band at 435 nm and 3 Q-bands between 525 and 665 nm. After metalation, the UV-vis spectrum of CoTAPP displays the expected loss of a Q-band.

The University of Texas at El Paso, 500 W University Ave., El Paso, TX, 79968, USA.
E-mail: dino@utep.edu

† Electronic supplementary information (ESI) available. See DOI: <https://doi.org/10.1039/d5dt01390a>

Electrografting of H₂TPP and CoTPP was carried out following the reported procedures with some modifications.^{22,23} The experiment was performed in a 10 mL electrochemical cell using a three-electrode setup (Ag/AgCl as reference electrode, platinum mesh counter electrode, and GCE working electrode). For the electrografting of H₂TPP-GCE, a solution containing 0.1 M HCl, 0.5 mM H₂TAPP, and 0.5 mM NaNO₂ was used. NaNO₂ was first dissolved in 0.1 M HCl, and this solution was then used to dissolve H₂TAPP while stirring under nitrogen gas for 10 min. The electrografting was conducted at a scan rate of 50 mV s⁻¹ in the potential range from 0.2 to -0.4 V vs. Ag/AgCl. For the CoTPP-GCE, 1.2 mM CoTAPP was dissolved in 0.5 mL DMF and 0.5 mL of acetonitrile and sonicated to ensure complete dissolution. Under an inert nitrogen atmosphere, the prepared solution was combined with a 100 μL NaNO₂ solution (1.4 mg in 20 μL DI water and 80 μL acetonitrile) which was added dropwise. After purging for 15 minutes, 0.1 M of tetrabutylammonium tetrafluoroborate (TBATFB) in acetonitrile (830 μL) along with trifluoroacetic (TFA) (170 μL) was added and stirred for 5 minutes under nitrogen. The electrografting was then performed at a scan rate of 50 mV s⁻¹ in the potential range of -0.4 to -0.85 V vs. Ag/AgCl.

The topography of H₂TPP-modified GCE was examined using atomic force microscopy (AFM), as shown in Fig. 1, revealing an average surface thickness of approximately 74 nm. Additionally, X-ray photoelectron spectroscopy (XPS) surveys (Fig. S3 and S4†) indicate that H₂TPP-GCE is composed of carbon and nitrogen, while CoTPP-GCE contains carbon, nitrogen, and cobalt. The high-resolution XPS spectrum of H₂TPP (Fig. S3†) shows N 1s peaks corresponding to pyrrolic nitrogen bonding. In contrast, the CoTPP spectrum (Fig. S4†) displays N 1s peaks associated with Co-N coordination, further confirmed by the Co 2p region, which exhibits two main peaks at binding energies of 780 and 795 eV, characteristic of Co²⁺.

The *in situ* generation and electrochemical reduction of porphyrin-diazonium salts requires low reduction potentials to generate the reactive species (*e.g.*, free radicals, Por[•]) which can readily attach to the glassy carbon surface.^{24,25}

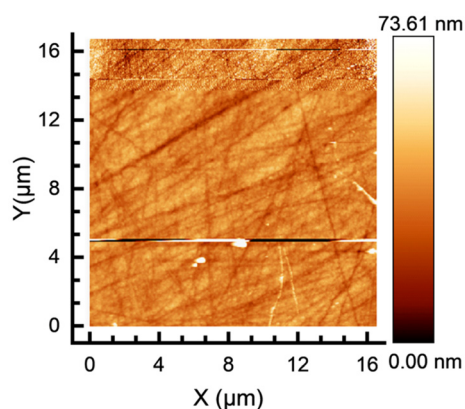
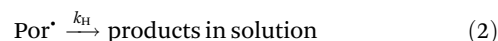


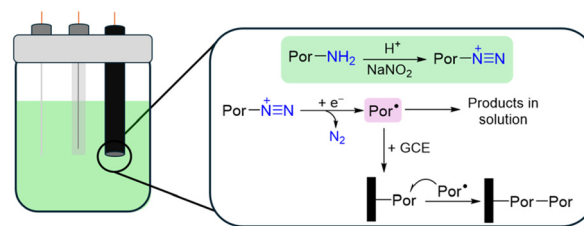
Fig. 1 Atomic force micrograph of H₂TPP-GCE. The film thickness is approximately 70 nm.

Additionally, the anchored molecules can continuously react with Por[•] giving rise to multi-layered films.²⁶ As depicted in Scheme 1, the covalent binding of both H₂TPP and CoTPP to the glassy carbon surface was performed by cyclic voltammetry (CV). Fig. S5† shows the CV cycles of 0.5 mM H₂TAPP as diazonium salt. After the first cycle, cathodic peaks at -0.07 V and -0.15 V vs. Ag/AgCl are observed, which suggest electroactive film formation and reduction of the protonated porphyrin (H₂TAPP⁺).²⁷ After five cycles, a peak shift from -0.07 V to -0.215 V vs. Ag/AgCl and an increase in the current response are observed. The rise in voltammetric current and potential shift can be associated with the build-up of the electropolymerized H₂TPP.²⁸ By repeating the cycling around the cathodic potential range leads to the reduction of the functional group and electroactive polymer deposition. In the case of CoTPP electrografting, Fig. S6† shows an irreversible electrochemical reduction process (peak Ic) at -0.73 V vs. Ag/AgCl, corresponding to the reduction of the CoTPP diazonium salt. After 25 consecutive cycles, the faradaic current decreased until it reached a baseline level. This suggests the electrogeneration of reactive intermediates that covalently bond to the glassy carbon surface which leads to the formation of a CoTPP thin film on GCE. The electrografting of both H₂TPP and CoTPP was also performed using the diazonium linker, formed *in situ* from the *para*-amino phenyl group of the porphyrin ring. This strategy allows for the covalent attachment through carbon-carbon coupling between the aryl moiety and the carbon surface.^{25,29} The only distinction between H₂TPP and CoTPP is the presence of Co with no significant structural differences between them.

We investigated the competition between electrode inhibition and coupled chemical reactions of the electrogenerated CoTPP porphyrin radical (Por[•]), following reactions eqn (1) and (2).



The Por[•] intermediate can either graft to the electrode surface or react in solution. Electrode inhibition is governed by the heterogeneous grafting rate constant (k_A), while the solution-phase reaction is described by the homogeneous rate constant (k_H). The model tracks fractional surface coverage (θ_n



Scheme 1 Electrografting experiment of H₂TAPP and CoTAPP on glassy carbon electrodes by the *in situ* generation of diazonium salts.

and θ_{n-1}) across cycles, approaching a current near zero as shown in eqn (3):²⁴

$$\theta_n = \theta_{n-1}^* + p \int_0^\tau (1 - \theta_n) \Psi^0 d\eta \quad (3)$$

This equation relates the dimensionless current Ψ^0 (in the absence of inhibition) and parameter p , which quantifies competition between surface and solution reactions³⁰ shown in eqn (4):

$$p = \frac{k_A}{k_A + \sqrt{Dk_H}} \frac{C^0}{\Gamma^0} \sqrt{\frac{RTD}{\alpha Fv}} \quad (4)$$

Using: $\alpha = 0.62$, $D = 10^{-5}$ cm² s⁻¹, $\Gamma^0 = 20 \times 10^{-10}$ mol cm⁻² we calculated $p = 0.92$, indicating that 92% of Por^r graft to the electrode, while 8% react in solution.

The electrografted layers of H₂TPP and CoTPP on GCE were studied in a 4 mM [Fe(CN)₆]^{3-/4-} solution as a redox probe. Fig. S7 and S8† show the cyclic voltammogram of the bare GCE, which corresponds to an electrochemically reversible system. Upon electrografting, the CV response of both H₂TPP-GCE and CoTPP-GCE lack the anodic and cathodic peaks, instead, exhibiting a capacitive current response suggesting the presence of chemisorbed films covering the GCE. The interface of H₂TPP-GCE and CoTPP-GCE was studied by electrochemical impedance spectroscopy (EIS), as shown in Fig. S9 and S10.† The Nyquist plot for bare GCE shows a semi-circle corresponding to the electron-transfer reaction next to a 45° back slope suggesting a diffusion-controlled system.³¹ H₂TPP-GCE and CoTPP-GCE depict an incomplete loop with a larger diameter, indicating the presence of chemisorbed species on the surface of the electrode that hinders the charge transfer process. EIS parameters were modelled using a Randles equivalent circuit and a double-circuit (Fig. S11†) to measure the dielectric effects of the H₂TPP and CoTPP layers on the GCE surface (Table S1†). The surface coverage of the GCE surface coated with H₂TPP and CoTPP films was calculated by comparing the charge transfer resistance (R_{ct}) values of the unmodified GCE (R_{ct}^0) and the modified GCE (R_{ct}'), as shown in equation:

$$\theta = 1 - \frac{R_{ct}^0}{R_{ct}'} \quad (5)$$

The calculated θ value is 99.9% and 98.3% for H₂TPP-GCE and CoTPP-GCE, respectively which shows the efficiency of this surface electrografting method.

The performance of the modified electrodes during HER was tested in a 0.5 M H₂SO₄ solution. Prior to use, the electrodes were pretreated by performing 15 CV cycles at a scan rate of 100 mV s⁻¹. The LSV curves in Fig. 2a show that H₂TPP-GCE exhibits a higher current response ($j = 51.5$ mA cm⁻²) and lower overpotential ($\eta_{10} = 511$ mV, where η_{10} is the overpotential at $j = 10$ mA cm⁻²) when compared to the bare GCE. The H₂TPP-GCE has an HER Tafel slope of 113 mV dec⁻¹ which is significantly lower than that of the bare GCE 342 mV dec⁻¹ (Fig. S12†) suggesting a Volmer–Heyrovsky mechanism.³² The

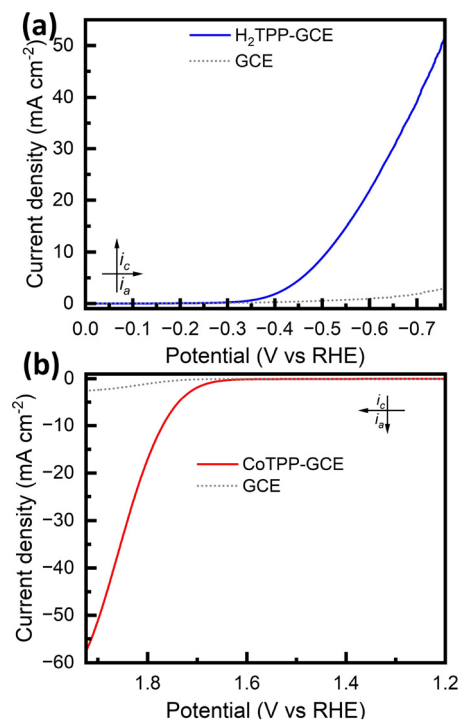


Fig. 2 Linear sweep voltammetry at a scan rate of 50 mV s⁻¹ in 0.5 M H₂SO₄ for HER, and 1 M KOH for OER. (a) HER LSV. (b) OER LSV.

CoTPP-modified electrode was also tested under identical HER conditions (Fig. S13a†); however, it exhibited negligible catalytic response, with a current density of only 3.82 mA cm⁻². Therefore, no further experiments were conducted for this electrode under HER conditions. The charge transfer resistance of H₂TPP-GCE Fig. 4a measured with EIS is 98 kΩ, which is also much lower than the bare electrode (718 kΩ) indicating enhanced conductivity of the electrografted film.

OER measurements were evaluated in 1 M KOH solution following a pretreatment step, during which 30 CV cycles were performed at a scan rate of 100 mV s⁻¹ prior LSV measurements. Fig. 2b demonstrates that CoTPP-GCE has a smaller η_{10} 540 mV and an improved current response (57 mA cm⁻²) compared to bare GCE. The Tafel slope in Fig. S14† demonstrated that CoTPP-GCE has fast catalytic kinetics (80 mV dec⁻¹) which is comparable with reported OER materials.^{29,33–37} The H₂TPP-GCE (Fig. S13b†) exhibits an overpotential of 650 mV and a current density of 13 mA cm⁻², which is significantly lower than that of CoTPP-GCE, indicating that the metal-free porphyrin polymer has poor OER activity. This reduced performance is attributed to the linker connecting the free-base porphyrin units in the polymer. This highlights our previous work, which demonstrated that the nature of the linker plays a critical role in determining the OER activity of metal-free porphyrin polymers.^{9,38}

To investigate the overall water splitting reaction, a three-electrode setup was employed in which CoTPP-GCE served as the working electrode and H₂TPP-GCE was used as the counter electrode, with the OER experiment shown in Fig. 3. The CV

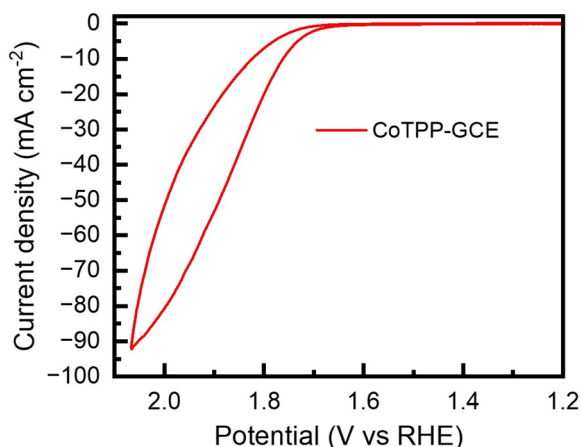


Fig. 3 Overall water splitting in 1.0 M KOH in a three-electrode configuration (CoTPP-GCE – working electrode, H₂TPP-GCE counter electrode, Hg/HgO alkaline reference electrode).

measurement revealed improved reaction kinetics, as evidenced by a significantly enhanced current response. Additionally, under these conditions the η_{10} was 532 mV, indicating that the combined use of both modified electrodes benefits the overall water splitting performance. The EIS in KOH solution (Fig. 4b) shows that CoTPP-GCE has a significantly smaller semicircle 44.2 Ω , compared to bare GCE (1.38 k Ω), indicating an enhanced electron transfer upon modification of the electrode.

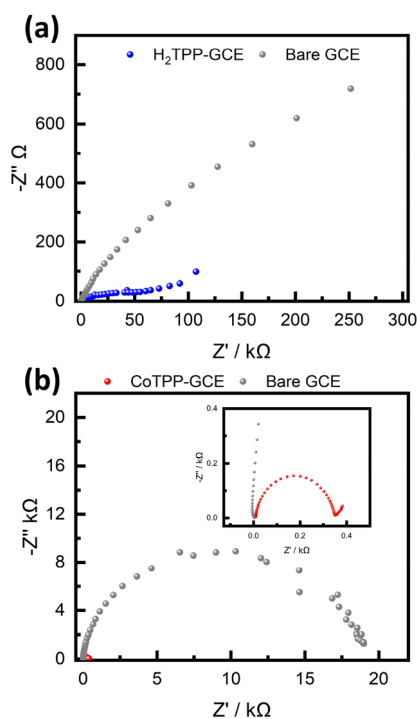


Fig. 4 Study of the charge transfer kinetics through Electrochemical Impedance Spectroscopy (EIS). (a) In 0.5 M H₂SO₄ and (b) in 1 M KOH.

The ionic mobility in the modified surfaces was evaluated by measuring the double-layer capacitance (C_{dl}) of H₂TPP-GCE and CoTPP-GCE. Fig. S15 and S16† show the CV curves in the non-faradaic region, while Fig. 5a and b illustrate the linear correlation of current density (j) with scan rate (ν) used to determine C_{dl} . In 0.5 M H₂SO₄, H₂TPP-GCE has a C_{dl} of 1.672 mF, compared to 0.340 mF for bare GCE, while in 1 M KOH, CoTPP-GCE has 1.167 mF, compared to 0.5123 mF of the bare GCE. Since C_{dl} is proportional to the electrochemically active surface area (ECSA), H₂TPP-GCE and CoTPP-GCE show significantly higher ECSA values (47.7 cm² and 29.2 cm², respectively) than bare GCE (9.72 cm² and 12.83 cm²).

Chronoamperometry experiments were conducted to assess the stability of the electrografted films. Both H₂TPP-GCE and CoTPP-GCE maintain stable currents over a 20 h period, in acid and basic conditions, respectively (Fig. S17 and S18†) with faradaic efficiencies of 90%. To benchmark the catalytic performance of H₂TPP-GCE and CoTPP-GCE, the turnover number (TON) and turnover frequency (TOF) were calculated using eqn (6) and (7):

$$\text{TON} = \text{TOF} \times t \quad (6)$$

$$\text{TOF} = \frac{j}{nC_{dl}\Delta V} \quad (7)$$

The TON, shown in eqn (6), measures the total amount of reactant molecules converted into products by a single catalyst molecule before it is consumed.³⁹ Here t denotes duration of the controlled potential bulk electrolysis experiment. The TOF,

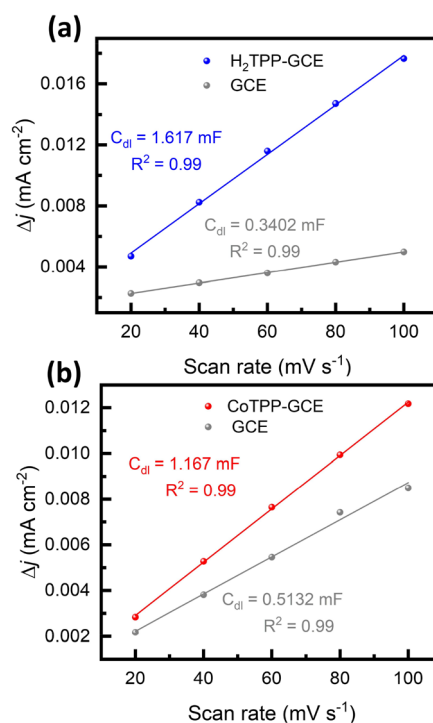


Fig. 5 Δj plotted against different scan rates yielding the double layer capacitance (C_{dl}). (a) In 0.5 M H₂SO₄ and (b) in 1.0 M KOH.

illustrated in eqn (7), reflects the catalytic activity by quantifying the amount of reactant transformed into products per catalyst site per unit of time. Given that the porphyrin layer is expected to be in the vicinity of the electrode surface, within Inner Helmholtz Plane, the number of active sites can be estimated from the C_{di} values. In this context, j is the average current density ($A\ cm^{-2}$) recorded during the bulk electrolysis experiment, n is the number of electrons involved in the overall reaction ($n = 2$ for HER, and $n = 4$ for OER), and ΔV is the potential window (V) used to determine C_{di} within the non-faradaic region employed.⁴⁰ In acidic media, H₂TPP-GCE exhibits a TON over 20 h of 21 960 and a TOF of 0.305 s⁻¹, and CoTPP-GCE a TON of 48 096 and a TOF of 0.668 s⁻¹ in basic media.

Conclusions

In summary, we successfully electrografted metal-free porphyrin (H₂TAPP) and cobalt porphyrin (CoTAPP) onto GCE *via in situ* diazonium salt formation and electropolymerization, enhancing ECSA and charge transfer kinetics. This process stabilizes the porphyrins, creating a well-dispersed network of active sites that improves HER and OER efficiency. When used as both anode and cathode, the modified electrodes enhance overall water-splitting performance in KOH. These results highlight the stabilization of porphyrins and advancement of electrochemically modified electrodes, offering the potential for efficient water splitting technologies applications, and in electrocatalysis in general.

Experimental

Materials

Sodium nitrite (NaNO₂ > 97%), trifluoroacetic (C₂HF₃O₂), and tetrabutylammonium tetrafluoroborate (TBABF₄) were purchased from Sigma Aldrich. Acetonitrile (C₂H₃N), dimethylformamide (C₃H₇NO, 99.5%), and hydrochloric acid (HCl, 36%) were purchased from Fisher Scientific and used without further purification.

Electrochemical methods

All measurements were performed in a two-compartment electrochemical H-cell using a CHI760E potentiostat. A glassy carbon electrode (3 mm diameter) was used as working electrode, Ag/AgCl as reference electrode, platinum mesh counter electrode. Prior to the electrochemical modification, the glassy carbon electrodes were polished using 0.30 and 0.05 μm alumina slurr on microcloth pads. Later the electrodes were then ultrasonicated with DI water, ethanol, and acetone, then dried with N₂ gas.

Electrografting of CoTPP-GCE

The electrografting of CoTPP was carried out *via* a diazonium-based modification approach. For this purpose, 7 mg of

CoTAPP was dissolved in 0.5 mL DMF and 0.5 mL acetonitrile, followed by sonication for 5 minutes and stirring under an N₂ atmosphere for 10 minutes to ensure complete dissolution and prevent oxidation. Subsequently, 100 μL of an ice-cold NaNO₂ solution (1.4 mg in 20 μL DI water and 80 μL acetonitrile) was added dropwise and stirred under N₂ for 15 minutes, facilitating the conversion of amine-functionalized CoTAPP into its corresponding diazonium salt. Next, 170 μL trifluoroacetic acid was mixed with 830 μL of TBABF₄ in acetonitrile (36.2 M) and added to the reaction mixture to stabilize the diazonium ion. After stirring for 5 minutes, an additional 6 mL of TBABF₄ in acetonitrile (36.2 M) was introduced, and the final solution with 1.2 mM CoTPP radical was stirred for another 10 minutes under continuous N₂ purging. The electrografting process was performed using a three-electrode system consisting of an Ag/AgCl reference electrode, a Pt mesh counter electrode, and a glassy carbon working electrode (3 mm diameter). Cyclic voltammetry was applied to reduce the diazonium salt of the porphyrin, generating aryl radicals that covalently bonded to the glassy carbon electrode surface. The potential was scanned between -0.4 V and -0.85 V *vs.* Ag/AgCl for 25 cycles. The modified electrode was rinsed with DMF to remove any residual reagents and stored for further characterization.

Electrografting of H₂TPP-GCE

The electrografting of H₂TPP-GCE, was performed using a solution containing 0.1 M HCl, 0.5 mM of H₂TAPP and NaNO₂. The weighed NaNO₂ was dissolved in 0.1 M HCl, and this mixture (8 mL) was then used to dissolve H₂TAPP. Subsequently 2 mL of 0.1 M HCl were added to make a 10 mL total solution. The mixture was stirred under N₂ gas for 10 min. The electrografting was conducted using standard 3 electrode setup consisting of Ag/AgCl reference electrode, a Pt mesh counter electrode, and a glassy carbon working electrode (3 mm diameter) at a scan rate of 50 mV s⁻¹ in the potential range of 0.2 to -0.4 V *vs.* Ag/AgCl for 35 cycles.

Author contributions

Conceptualization and project administration – Neidy Ocuane, Nasim Jafari, Jonathan J. Calvillo Solis, Dino Villagrán. Methodology data curation and investigation – Neidy Ocuane, Nasim Jafari, Jonathan J. Calvillo Solis, Manuel Saucedo. Validation and resources – Dino Villagrán. Funding acquisition and supervision – Dino Villagrán. Writing – original draft – Neidy Ocuane. Review and editing – Neidy Ocuane Jonathan J. Calvillo, Nasim Jafari, Dino Villagrán.

Conflicts of interest

There are no conflicts to declare.

Data availability

The data supporting this article have been included as part of the ESI.†

Acknowledgements

We thank Dr Sreepasad T Sreenivasan and his student Kavish Saini for the AFM image. This work was supported by the Welch Foundation AH-2083-20240404 and partially supported by Cleantech FWP 100898 funded by the U.S. Department of Energy, Office of Science, Basic Energy Sciences. We want to acknowledge the financial support from NSF for the acquisition of the XPS equipment (NSF/CHEM 2216473).

References

- 1 A. F. Ferreira, A. C. Marques, A. P. Batista, P. A. S. S. Marques, L. Gouveia and C. M. Silva, Biological Hydrogen Production by *Anabaena* Sp. – Yield, Energy and CO₂ Analysis Including Fermentative Biomass Recovery, *Int. J. Hydrogen Energy*, 2012, **37**(1), 179–190, DOI: [10.1016/j.ijhydene.2011.09.056](https://doi.org/10.1016/j.ijhydene.2011.09.056).
- 2 A. Mehtab, S. A. Ali, I. Sadiq, S. Shaheen, H. Khan, M. Fazil, N. A. Pandit, F. Naaz and T. Ahmad, Hydrogen Energy as Sustainable Energy Resource for Carbon-Neutrality Realization, *ACS Sustainable Resour. Manage.*, 2024, **1**(4), 604–620, DOI: [10.1021/acssusresmg.4c00039](https://doi.org/10.1021/acssusresmg.4c00039).
- 3 A. M. Sadeq, R. Z. Homod, A. K. Hussein, H. Togun, A. Mahmoodi, H. F. Isleem, A. R. Patil and A. H. Moghaddam, Hydrogen Energy Systems: Technologies, Trends, and Future Prospects, *Sci. Total Environ.*, 2024, **939**, 173622, DOI: [10.1016/j.scitotenv.2024.173622](https://doi.org/10.1016/j.scitotenv.2024.173622).
- 4 F. Bellato, M. Ferri, A. Annamalai, M. Prato, L. Leoncino, R. Brescia, L. De Trizio and L. Manna, Colloidal Synthesis of Nickel Arsenide Nanocrystals for Electrochemical Water Splitting, *ACS Appl. Energy Mater.*, 2023, **6**(1), 151–159, DOI: [10.1021/acsaem.2c02698](https://doi.org/10.1021/acsaem.2c02698).
- 5 C. Wei, Z. Wang, K. Otani, D. Hochfilzer, K. Zhang, R. Nielsen, I. Chorkendorff and J. Kibsgaard, Benchmarking Electrocatalyst Stability for Acidic Oxygen Evolution Reaction: The Crucial Role of Dissolved Ion Concentration, *ACS Catal.*, 2023, **13**(21), 14058–14069, DOI: [10.1021/acscatal.3c03257](https://doi.org/10.1021/acscatal.3c03257).
- 6 Y. Liu, Y. Wang, H. Li, M. G. Kim, Z. Duan, K. Talat, J. Y. Lee, M. Wu and H. Lee, Effectiveness of Strain and Dopants on Breaking the Activity-Stability Trade-off of RuO₂ Acidic Oxygen Evolution Electrocatalysts, *Nat. Commun.*, 2025, **16**(1), 1717, DOI: [10.1038/s41467-025-56638-8](https://doi.org/10.1038/s41467-025-56638-8).
- 7 A. Fatima, H. Aldosari, M. S. Al-Buriahi, M. Al Huwayz, Z. A. Alrowaili, M. S. Alqahtani, M. Ajmal, A. Nazir, M. Iqbal, R. Tur Rasool, S. Muqaddas and A. Ali, Cobalt Ferrite Surface-Modified Carbon Nanotube Fibers as an Efficient and Flexible Electrode for Overall Electrochemical Water Splitting Reactions, *ACS Omega*, 2023, **8**(41), 37927–37935, DOI: [10.1021/acsomega.3c03314](https://doi.org/10.1021/acsomega.3c03314).
- 8 N. Ocuane, Y. Ge, C. Sandoval-Pauker and D. Villagrán, Bifunctional Porphyrin-Based Metal–Organic Polymers for Electrochemical Water Splitting, *Dalton Trans.*, 2024, **53**(5), 2306–2317, DOI: [10.1039/D3DT03371F](https://doi.org/10.1039/D3DT03371F).
- 9 Y. Ge, Z. Lyu, M. Marcos-Hernández and D. Villagrán, Free-Base Porphyrin Polymer for Bifunctional Electrochemical Water Splitting, *Chem. Sci.*, 2022, **13**(29), 8597–8604, DOI: [10.1039/D2SC01250B](https://doi.org/10.1039/D2SC01250B).
- 10 Y. Wu, N. Rodríguez-López and D. Villagrán, Hydrogen Gas Generation Using a Metal-Free Fluorinated Porphyrin, *Chem. Sci.*, 2018, **9**(20), 4689–4695, DOI: [10.1039/C8SC00093J](https://doi.org/10.1039/C8SC00093J).
- 11 L. Smykalla, P. Shukryna, C. Mende, H. Lang, M. Knupfer and M. Hietschold, Photoelectron Spectroscopy Investigation of the Temperature-Induced Deprotonation and Substrate-Mediated Hydrogen Transfer in a Hydroxyphenyl-Substituted Porphyrin, *Chem. Phys.*, 2015, **450–451**, 39–45, DOI: [10.1016/j.chemphys.2015.02.001](https://doi.org/10.1016/j.chemphys.2015.02.001).
- 12 X. Li, H. Lei, L. Xie, N. Wang, W. Zhang and R. Cao, Metalloporphyrins as Catalytic Models for Studying Hydrogen and Oxygen Evolution and Oxygen Reduction Reactions, *Acc. Chem. Res.*, 2022, **55**(6), 878–892, DOI: [10.1021/acs.accounts.1c00753](https://doi.org/10.1021/acs.accounts.1c00753).
- 13 B. Wurster, D. Grumelli, D. Hötger, R. Gutzler and K. Kern, Driving the Oxygen Evolution Reaction by Nonlinear Cooperativity in Bimetallic Coordination Catalysts, *J. Am. Chem. Soc.*, 2016, **138**(11), 3623–3626, DOI: [10.1021/jacs.5b10484](https://doi.org/10.1021/jacs.5b10484).
- 14 J. H. Zagal, S. Griveau, J. F. Silva, T. Nyokong and F. Bedioui, Metallophthalocyanine-Based Molecular Materials as Catalysts for Electrochemical Reactions, *Coord. Chem. Rev.*, 2010, **254**(23–24), 2755–2791, DOI: [10.1016/j.ccr.2010.05.001](https://doi.org/10.1016/j.ccr.2010.05.001).
- 15 I. Barraza Alvarez, Y. Wu, J. Sanchez, Y. Ge, M. V. Ramos-Garcés, T. Chu, T. F. Jaramillo, J. L. Colón and D. Villagrán, Cobalt Porphyrin Intercalation into Zirconium Phosphate Layers for Electrochemical Water Oxidation, *Sustainable Energy Fuels*, 2021, **5**(2), 430–437, DOI: [10.1039/D0SE01134G](https://doi.org/10.1039/D0SE01134G).
- 16 L. Wang, L. Wang, X. Meng and F. Xiao, New Strategies for the Preparation of Sinter-Resistant Metal–Nanoparticle-Based Catalysts, *Adv. Mater.*, 2019, **31**(50), 1901905, DOI: [10.1002/adma.201901905](https://doi.org/10.1002/adma.201901905).
- 17 L. Qian, S. Luo, L. Wu, X. Hu, W. Chen and X. Wang, In Situ Growth of Metal Organic Frameworks Derived Hierarchical Hollow Porous Co₃O₄/NiCo₂O₄ Nanocomposites on Nickel Foam as Self-Supported Flexible Electrode for Methanol Electrocatalytic Oxidation, *Appl. Surf. Sci.*, 2020, **503**, 144306, DOI: [10.1016/j.apsusc.2019.144306](https://doi.org/10.1016/j.apsusc.2019.144306).
- 18 L. Wang, D. Jia, L. Yue, K. Zheng, A. Zhang, Q. Jia and J. Liu, In Situ Fabrication of a Uniform Co-MOF Shell

- Coordinated with CoNiO₂ to Enhance the Energy Storage Capability of NiCo-LDH via Vapor-Phase Growth, *ACS Appl. Mater. Interfaces*, 2020, **12**(42), 47526–47538, DOI: [10.1021/acscami.0c12759](https://doi.org/10.1021/acscami.0c12759).
- 19 R. W. Murray, Chemically Modified Electrodes, *Acc. Chem. Res.*, 1980, **13**(5), 135–141, DOI: [10.1021/ar50149a002](https://doi.org/10.1021/ar50149a002).
- 20 R. M. Bullock, A. K. Das and A. M. Appel, Surface Immobilization of Molecular Electrocatalysts for Energy Conversion, *Chem. – Eur. J.*, 2017, **23**(32), 7626–7641, DOI: [10.1002/chem.201605066](https://doi.org/10.1002/chem.201605066).
- 21 M. Malakzadeh, J. B. Raoof, A. Ghafarnejad and R. Ojani, In situ Electrosynthesis Cu-PtBTC MOF-Derived Nanocomposite Modified Glassy Carbon Electrode for Highly Performance Electrocatalysis of Hydrogen Evolution Reaction, *J. Electroanal. Chem.*, 2021, **900**, 115716, DOI: [10.1016/j.jelechem.2021.115716](https://doi.org/10.1016/j.jelechem.2021.115716).
- 22 F. Mo, D. Qiu, L. Zhang and J. Wang, Recent Development of Aryl Diazonium Chemistry for the Derivatization of Aromatic Compounds, *Chem. Rev.*, 2021, **121**(10), 5741–5829, DOI: [10.1021/acs.chemrev.0c01030](https://doi.org/10.1021/acs.chemrev.0c01030).
- 23 S. Hebié, A. K. D. Dimé, C. H. Devillers and D. Lucas, Electrochemistry as an Attractive and Effective Tool for the Synthesis and Immobilization of Porphyrins on an Electrode Surface, *Chem. – Eur. J.*, 2015, **21**(22), 8281–8289, DOI: [10.1002/chem.201404314](https://doi.org/10.1002/chem.201404314).
- 24 D. Morales-Martínez and F. J. González, A Mechanistic Approach to the Electrografting of Carbon Surfaces and Electrochemical Properties of the Grafted Films – A Critical Review, *Electrochim. Acta*, 2022, **425**, 140693, DOI: [10.1016/j.electacta.2022.140693](https://doi.org/10.1016/j.electacta.2022.140693).
- 25 Z. Kudas, U. Atmaca, T. Saruhan, M. Celik and D. Ekinci, Electrocatalytic Reduction of Oxygen at Glassy Carbon Electrodes Coated with Diazonium-derived Porphyrin/Metalloporphyrin Films, *Electroanalysis*, 2020, **32**(6), 1379–1390, DOI: [10.1002/elan.201900707](https://doi.org/10.1002/elan.201900707).
- 26 R. L. McCreery, Advanced Carbon Electrode Materials for Molecular Electrochemistry, *Chem. Rev.*, 2008, **108**(7), 2646–2687, DOI: [10.1021/cr068076m](https://doi.org/10.1021/cr068076m).
- 27 H. M. Castro-Cruz and N. A. Macías-Ruvalcaba, Electroreduction Mechanisms of *Meso*-Tetraphenylphlorin Cation in Strongly Acidic Media of Benzonitrile, *J. Electroanal. Chem.*, 2024, **961**, 118220, DOI: [10.1016/j.jelechem.2024.118220](https://doi.org/10.1016/j.jelechem.2024.118220).
- 28 S. Griveau, V. Albin, T. Pauporté, J. H. Zagal and F. Bedioui, Comparative Study of Electropolymerized Cobalt Porphyrin and Phthalocyanine Based Films for the Electrochemical Activation of Thiols, *J. Mater. Chem.*, 2002, **12**(2), 225–232, DOI: [10.1039/b106817b](https://doi.org/10.1039/b106817b).
- 29 T. M. T. Huynh and T. H. Phan, Covalent Molecular Anchoring of Metal-Free Porphyrin on Graphitic Surfaces toward Improved Electrocatalytic Activities in Acidic Medium, *Coatings*, 2024, **14**(6), 745, DOI: [10.3390/coatings14060745](https://doi.org/10.3390/coatings14060745).
- 30 P. Allongue, M. Delamar, B. Desbat, O. Fagebaume, R. Hitmi, J. Pinson and J.-M. Savéant, Covalent Modification of Carbon Surfaces by Aryl Radicals Generated from the Electrochemical Reduction of Diazonium Salts, *J. Am. Chem. Soc.*, 1997, **119**(1), 201–207, DOI: [10.1021/ja963354s](https://doi.org/10.1021/ja963354s).
- 31 J. Huang, Diffusion Impedance of Electroactive Materials, Electrolytic Solutions and Porous Electrodes: Warburg Impedance and Beyond, *Electrochim. Acta*, 2018, **281**, 170–188, DOI: [10.1016/j.electacta.2018.05.136](https://doi.org/10.1016/j.electacta.2018.05.136).
- 32 T. Shinagawa, A. T. Garcia-Esparza and K. Takanebe, Insight on Tafel Slopes from a Microkinetic Analysis of Aqueous Electrocatalysis for Energy Conversion, *Sci. Rep.*, 2015, **5**(1), 13801, DOI: [10.1038/srep13801](https://doi.org/10.1038/srep13801).
- 33 S. K. Das, A. Chowdhury, K. Bhunia, A. Ghosh, D. Chakraborty, M. Das, U. Kayal, A. Modak, D. Pradhan and A. Bhaumik, Ni(II) and Cu(II) Grafted Porphyrin-Pyrene Based Conjugated Microporous Polymers as Bifunctional Electrocatalysts for Overall Water Splitting, *Electrochim. Acta*, 2023, **459**, 142553, DOI: [10.1016/j.electacta.2023.142553](https://doi.org/10.1016/j.electacta.2023.142553).
- 34 A. N. Marianov and Y. Jiang, Effect of Manganese Porphyrin Covalent Immobilization on Electrocatalytic Water Oxidation and Oxygen Reduction Reactions, *ACS Sustainable Chem. Eng.*, 2019, **7**(4), 3838–3848, DOI: [10.1021/acssuschemeng.8b04735](https://doi.org/10.1021/acssuschemeng.8b04735).
- 35 Y. Wang, D. Song, J. Li, Q. Shi, J. Zhao, Y. Hu, F. Zeng and N. Wang, Covalent Metalloporphyrin Polymer Coated on Carbon Nanotubes as Bifunctional Electrocatalysts for Water Splitting, *Inorg. Chem.*, 2022, **61**(26), 10198–10204, DOI: [10.1021/acs.inorgchem.2c01415](https://doi.org/10.1021/acs.inorgchem.2c01415).
- 36 D. Bansal, D. Cardenas-Morcoso and N. Boscher, Conjugated Porphyrin Polymer Films with Nickel Single Sites for the Electrocatalytic Oxygen Evolution Reaction, *J. Mater. Chem. A*, 2023, **11**(10), 5188–5198, DOI: [10.1039/D2TA07748E](https://doi.org/10.1039/D2TA07748E).
- 37 S. Sarkar, S. Behera, R. Munjal, A. Chakraborty, B. Mondal and S. Mukhopadhyay, Non-Noble-Metal-Based Porphyrin Covalent Organic Polymers as Additive-/Annealing-Free Electrocatalysts for Water Splitting and Biomass Oxidation, *Energy Fuels*, 2024, **38**(6), 5183–5191, DOI: [10.1021/acs.energyfuels.4c00029](https://doi.org/10.1021/acs.energyfuels.4c00029).
- 38 Y. Ge, N. Ocuane, A. Denning, Y. Wu, J. Sanchez, M. V. Ramos-Garcés, J. Colón, T. F. Jaramillo and D. Villagran, Metalloporphyrin Organic Polymers as Effective and Stable Electrocatalysts for the Oxygen and Hydrogen Evolution Reactions, *SSRN*, 2025, preprint, DOI: [10.2139/ssrn.5280730](https://doi.org/10.2139/ssrn.5280730).
- 39 C. Costentin, G. Passard and J.-M. Savéant, Benchmarking of Homogeneous Electrocatalysts: Overpotential, Turnover Frequency, Limiting Turnover Number, *J. Am. Chem. Soc.*, 2015, **137**(16), 5461–5467, DOI: [10.1021/jacs.5b00914](https://doi.org/10.1021/jacs.5b00914).
- 40 Z. Weng, J. Jiang, Y. Wu, Z. Wu, X. Guo, K. L. Materna, W. Liu, V. S. Batista, G. W. Brudvig and H. Wang, Electrochemical CO₂ Reduction to Hydrocarbons on a Heterogeneous Molecular Cu Catalyst in Aqueous Solution, *J. Am. Chem. Soc.*, 2016, **138**(26), 8076–8079, DOI: [10.1021/jacs.6b04746](https://doi.org/10.1021/jacs.6b04746).